ADVANCED MATERIALS
www.advmat.de

A General Crosslinker Strategy to Realize Intrinsic Frozen Resistance of Hydrogels

*Dong Zhang, Yonglan Liu, Yanghe Liu, Yipeng Peng, Yijing Tang, Liming Xiong, Xiong Gong, and Jie Zheng**

Development and understanding of antifreezing materials are fundamentally and practically important for materials design and delivery. However, almost all of antifreezing materials are either organic/icephobic materials containing no water or hydrophilic hydrogels containing antifreezing additives. Here, a general crosslinking strategy to fabricate a family of EGINA-crosslinked double-network hydrogels with intrinsic, built-in antifreezing and mechanical properties, but without any antifreezing additives is proposed and demonstrated. The resultant hydrogels, despite large structural and compositional variations of hydrophilies, electrolytes, zwitterions, and macromolecules of polymer chains, achieved strong antifreezing and mechanical properties in different environments including solution state, gel state, and hydrogel/solid interfaces. Such general antifreezing property of EGINA-crosslinked hydrogels, regardless network compositions, is likely stemmed from their highly hydrophilic and tightly crosslinked DN structures for inducing strong water–network bindings to prevent ice crystal formation from free waters in hydrogel networks. EGINA-crosslinked hydrogels can also serve as a key component to be fabricated into smart windows with high optical transmittance and supercapacitors with excellent electrochemical stability at subzero temperatures. This work provides a simple, blueprint antifreezing design concept and a family of antifreezing hydrogels for the better understanding of the composite–structure–property relationship of antifreezing materials and the fundamentals of confined water in wet soft materials.

1. Introduction

Icing as a ubiquitous natural phenomenon is fundamentally important for all life on earth, but undesired icing has a long history of causing severe economic, environmental, and life-threatening issues.[1,2] To address this grand challenge, there has been considerable interests in developing different antifreezing (anti-icing) materials and strategies, simply because the extremely antifreezing property has significant impacts on fundamental concepts of materials designs and icing/anti-icing mechanisms, as well as many practical applications for wearable devices, energy storage electronics, artificial tissues, and human–machine interfaces.[3] Traditional antifreezing materials are dry, contain no water (e.g., superhydrophobic materials,[4] elastomers,[5] and organogels[6,7]), and have been studied extensively. But, these dry antifreezing materials often suffer from several limits,[8] for example, they often lose their antifreezing property upon exposure to wet environments, lack mechanical properties in cold conditions due to ease of solidification, and form unstable and brittle antifreezing coatings due to weak surface adhesion.

Recently, hydrogels have been considered and developed into new and emerging antifreezing materials, because hydrogels possess additional advantages of soft-tissue biomimics, hybrid liquid–solid properties, porous structure for small molecule transport, and surface adhesion.[9] On the other hand, in contrast to traditional antifreezing materials containing no water, it has proved extremely challenging, from materials design to delivery, for developing water-rich antifreezing hydrogels. Conventional design wisdom prevents a large amount of water (50–95%) and antifreezing function to be both presented in the same materials. Current antifreezing strategies are to incorporate different antifreezing additives of 1) ionic compounds (NaCl, $ZnCl_2$, $CaCl_2$, ionic liquids),[10,11] 2) natural biomolecules (antifreeze proteins, ice-binding proteins, glycoproteins, and silk proteins),[12,13] 3) carbon/nano materials (carbon nanotubes, nanofillers, oleophilic materials),[6,14] and 4) organic/water solvent (DMSO, benzyltrimethyl ammonium hydroxide, betaine, proline, glycerol)[15] into polymer networks, which helps to shift the water–ice phase equilibrium at different

D. Zhang, Y. Liu, Y. Tang, J. Zheng
Department of Chemical
Biomolecular
and Corrosion Engineering
The University of Akron
Akron, OH 44325, USA
E-mail: zhengj@uakron.edu
Y. Liu, X. Gong
School of Polymer Science and Polymer Engineering
College of Engineering and Polymer Science
The University of Akron
Akron, OH 44325, USA
Y. Peng, L. Xiong
Department of Aerospace Engineering
Iowa State University
Ames, IA 50010, USA
The ORCID identification number(s) for the author(s) of this article can be found under https://doi.org/10.1002/adma.202104006.

DOI: 10.1002/adma.202104006

stages of ice condensation, nucleation, and growth.[12] Another profound challenge of these antifreezing hydrogels is lacking mechanical properties even at room temperatures. Additionally, it should be noted that when incorporating antifreezing additives to soluble polymer networks, they are largely considered as organogels (i.e., organo/hydro gels), but not hydrogels. Surprisingly, there is a remarkable lack of development of pure polymeric antifreezing hydrogels without any antifreezing additive. Currently, only ethylene glycol-based waterborne anionic polyurethane acrylates/polyacrylamide (EG-waPUA/PAM) hydrogel[16] was reported as a fully polymeric antifreezing hydrogel without adding any antifreezing additive, but such a single hydrogel system with a complex network structure makes it difficult to derive a general structural-dependent antifreezing mechanism. Thus, antifreezing hydrogels without antifreezing additives are still far from ideal.[17] High water content in hydrogels inevitably provides grand challenges/opportunities for the discovery of new antifreezing and tough materials, unusual antifreezing and mechanical phenomena, and novel antifreezing and toughening mechanisms under super-cold and deformation conditions.

In this work, we designed and explored a new family of antifreezing hydrogels without adding any antifreezing additives, all of which were able to achieve intrinsic, built-in antifreezing and mechanical properties at −20 °C for hours in both aqueous solution and gel state. Since the resultant antifreezing polymers/hydrogels were prepared by a wide range of monomers ranging from hydrophilies, electrolytes, zwitterions, to macromolecules, crosslinked by 4,9-dioxo-5,8-dioxa-3,10-diazadodecane-1,12-diyl diacrylate (EGINA) and *N*,*N*′-methylenebis(acrylamide) (MBAA) and formed by two distinct single-network (SN) or double-network (DN) structures, they provide highly versatile compositional and structural parameters for better understanding the composition–structure–performance relationship of these antifreezing materials in different environments including solution state, gel state, and hydrogel/solid interfaces, in response to changes in polymer architectures, chemical pendant/terminal groups, network structures, and functional crosslinkers. The general antifreezing property of our hydrogels is likely stemmed from three synergistic design concepts: i) intrinsic, strong water-binding networks and crosslinkers; ii) tightly crosslinked and interpenetrating double-network structures with different energy dissipation modes; and iii) multiple antifreezing activities inside bulk hydrogels and at hydrogel–solid interface for preventing the ice formation at different stages. Finally, we applied gelatin/PHEAA and PVA/PAAm DN hydrogels separately to smart windows and supercapacitors for addressing the freezing-induced efficiency reduction. This work for the first time developed a new family of pure polymeric antifreezing hydrogels beyond the few available today, whose structural and compositional variations allow to explore their intrinsic antifreezing mechanisms.

2. Results and Discussion

2.1. Importance of EGINA Crosslinker for Antifreezing Polymer Solutions and Hydrogels

As a proof-of-concept, we designed and synthesized an ethyl glycol-derivative crosslinker of EGINA by coupling isocyanate and hydroxyl groups via a single-step additive reaction, whose chemical structure was verified by ^{1}H-NMR spectrum (Figure S3, Supporting Information). EGINA is designed as a water freezing inhibitor due to its similar structure to alcohol-like molecules. As compared to conventional crosslinker of MBAA, EGINA contains not only highly rich hydrogen bonding receptor/donator sites, but also symmetrical double bonds in both ends, allowing it to chemically and physically crosslink with polymer chains to form stable and unified networks. Quantitatively, we compared H-bond site, unsaturation degree (carbon–carbon double bonds), and hydrophilic factor between EGINA and MBAA using molecular simulations. Evidently, EGINA had the two-more-fold H-bond sites than MBAA, but comparable unsaturation degree and hydrophilic factor to MBAA (**Figure 1**a). This structural feature allows EGINA to i) engage strong interactions with both polymer networks and water molecules via hydrogen bonds, ii) facilitate the formation of chain clusters around the crosslinker sites, and iii) tune the space distance between adjacent polymer chains, all of which would promote the formation of strongly bound water with polymers and crosslinkers and competitively reduce the number of free water molecules inside hydrogels, thus preventing the formation of ice crystals. EGINA of 5 mol%, due to its low crosslinking efficiency, is equivalent to MBAA of 0.1 mol% for initiating and achieving the comparable gelation (Figure 1a, inset). To test EGINA-enhanced antifreezing effect, we prepared three different materials of crosslinker solution, PAAm (SN) hydrogel, and PVA/PAAm (DN) hydrogel in the presence of either EGINA or MBAA crosslinkers. In situ time-dependent microscopic images in Figure 1b showed that 5 wt% EGINA solution took ≈15 min to form observable ice crystals at −20 °C, whose frozen time was three times longer than that of 0.1 wt% MBAA solution (≈5 min). More interestingly, upon freezing, EGINA solution produced much smaller frozen-like bubbles than MBAA solution. Further TGA results confirmed that there were no strongly bound water molecules in both EGINA and MBAA solutions (Figure S4a, Supporting Information). Molecular dynamics (MD) simulations of EGINA and MBAA in explicit water molecules revealed that EGINA had the smaller Voronoi volume than MBAA (Figure 1c), indicating that EGINA has the stronger short-range interactions with surrounding water molecules, thus possibly affect the phase transition of free water in solution particularly at subzero temperatures.

In parallel, both EGINA-crosslinked PAAm SN and PVA/PAAm DN hydrogels exhibited the much stronger antifreezing property than both MBAA-crosslinked hydrogels, as evidenced by the longer frozen time and the non-observable ice crystallization. TGA data further showed that both EGINA-crosslinked SN and DN hydrogels had much slower weight loss than MBAA-crosslinked gels, indicating that EGINA imposes strong binding to surrounding water within polymer matrix so as to suppress the degradation of polymers and the loss of water (Figure S4b-d, Supporting Information).[11] DSC results showed that EGINA-crosslinked PVA/PAAm DN hydrogels had a freezing point of −27.5 °C, which was significantly lower than those of MBAA-crosslinked PVA/PAAm DN hydrogels (−23.8 °C), EGINA-crosslinked PAAm SN hydrogels (−21.5 °C), MBAA-crosslinked PAAm SN hydrogels (−19.8) (Figure 1d).

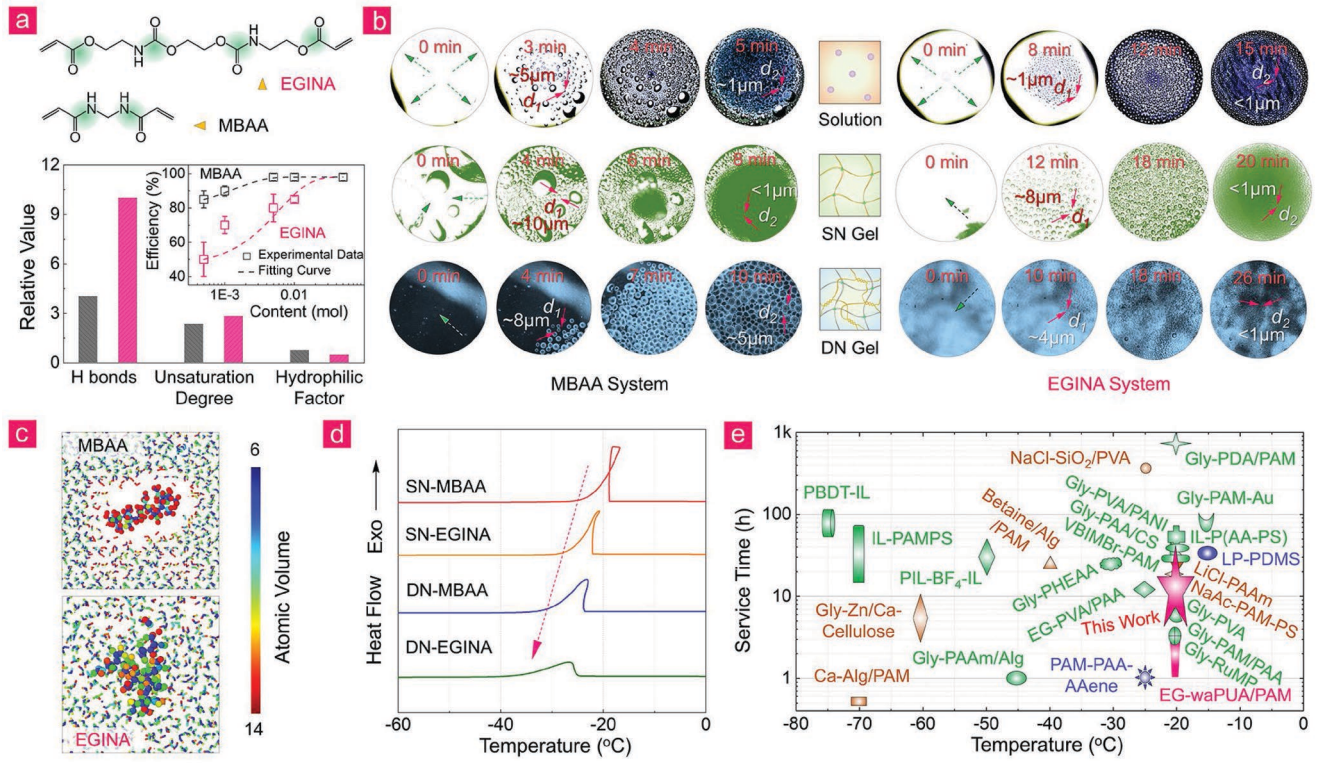

Figure 1. EGINA-crosslinking strategy for designing intrinsic polymeric antifreezing materials both in solution and gel states. a) Chemical structure, structural characterization (i.e., hydrogen bond sites, unsaturation degree, and hydrophilicity), and concentration-dependent crosslinking efficiency of MBAA and EGINA. b) In situ freezing process of EGINA- and MBAA-containing aqueous solution, EGINA- and MBAA-crosslinked PAAm SN and PVA/PAAm DN hydrogels. c) Comparison of atomic volume of MBAA and EGINA aqueous solution by LAMMPS with the CHARMM force field. d) DSC curves of EGINA- and MBAA-crosslinked PAAm SN and PVA/PAAm DN hydrogels between –60 and 25 °C. e) Comparison of the frozen-resistance performance (i.e., tolerance time and temperature) between hydrogels containing organic solvents (green dots),[18] hydrogels containing inorganic salts (brown dots),[19] elastomers/hydrogels (blue dots),[1,20] and pure hydrogels without any additives (red dots).[16]

Also, when incubating EGINA with BSA proteins at a wide range of temperatures from –8 to 8 °C, CD spectra clearly showed that the subzero temperatures did not affect the secondary structures of BSA proteins particularly at ≈200–210 nm (Figure S5, Supporting Information), suggesting that EGINA, from another viewpoint, demonstrates its protective role for proteins against cold-temperature-induced structural denaturation. Further MD simulations of PAAm polymers in the presence of EGINA or MBAA crosslinkers showed that EGINA-PAAm solution presented the smaller Voronoi volume and radial distribution function (RDF) values MBAA-PAAm solution (Figure S6, Supporting Information). The stretching and compressing MD dynamics results revealed that EGINA-PAAm polymers tended to experience the multiple early cracks and exhibited relatively higher tensile/compression stress than MBAA-PAAm polymers under the same strain conditions (Figures S7 and S8 and Videos S1 and S2, Supporting Information). These results confirm that EGINA can effectively inhibit the growth of ice nucleation by greatly reducing free water molecules, water–water interactions, and subsequent ice crystallization in both solution and gel states. The EGINA-induced antifreezing performance became more pronounced in DN hydrogels, probably because EGINA-crosslinked DN structures strengthen polymer–water interactions via hydrogen bonds, increase the number of tightly bound water, and thus lower the freezing points.

As a proof-of-concept, we summarized the frozen-resistance performance of our and other antifreezing hydrogels in terms of tolerated time (h) and tolerated temperature (°C) in Figure 1e and Table S1, Supporting Information. It can be seen that most of the antifreezing hydrogels were routinely prepared by incorporating either organic solvents (e.g., ethylene glycol, glycerin, and ionic liquids; as indicated by green dots) or inorganic salts (LiCl, NaCl, $CaCl_2$, and $ZnCl_2$; brown dots), all of which presented superior freezing tolerance up to ≈0.5–300 h under a wide range of temperature of ≈–20 to –75 °C. A few hybrid elastomer/hydrogel interfaces (blue dots) exhibited the better freezing resistance when applying to surface coatings. Different from those antifreezing organogels and elastomers/hydrogels, we demonstrated a simple crosslinking strategy to directly design pure polymeric antifreezing materials and hydrogels, which can achieve comparable freezing tolerance for ≈2–24 h at –20 °C without assistance from any antifreezing additives.

2.2. General Fabrication of Four Types of EGINA-Crosslinked Antifreezing DN Hydrogels

To prove our working hypothesis whether EGINA crosslinker could be generally applicable to other DN hydrogels by introducing the built-in antifreezing property, we designed and

synthesized four typical EGINA-crosslinked DN hydrogels, including PVA/PHEAA, gelatin/PHEAA, agar/PAAm, and BSA/PAAm hydrogels. These four EGINA-crosslinked DN hydrogels covered different combinations of both networks with rich amide, hydroxyl, carbonyl groups, that is, polysaccharides of agar, global protein of BSA and gelatin, and polymer of PVA as the first network, while hydrophilic PHEAA and PAAm as the second network. We have previously studied these four DN hydrogels for their mechanical and adhesive properties, but neither of them exhibited antifreezing property due to lack of EGINA crosslinkers. To test this hypothesis, at a first glance in **Figure 2**a and Video S3, Supporting Information, all EGINA-crosslinked DN hydrogels frozen at −20 °C for 24 h can be stretched up to ≈6–30 times their initial lengths without breaking, in sharp contrast to MBAA-crosslinked, frozen DN hydrogels that were easily broken even at a very low strain of

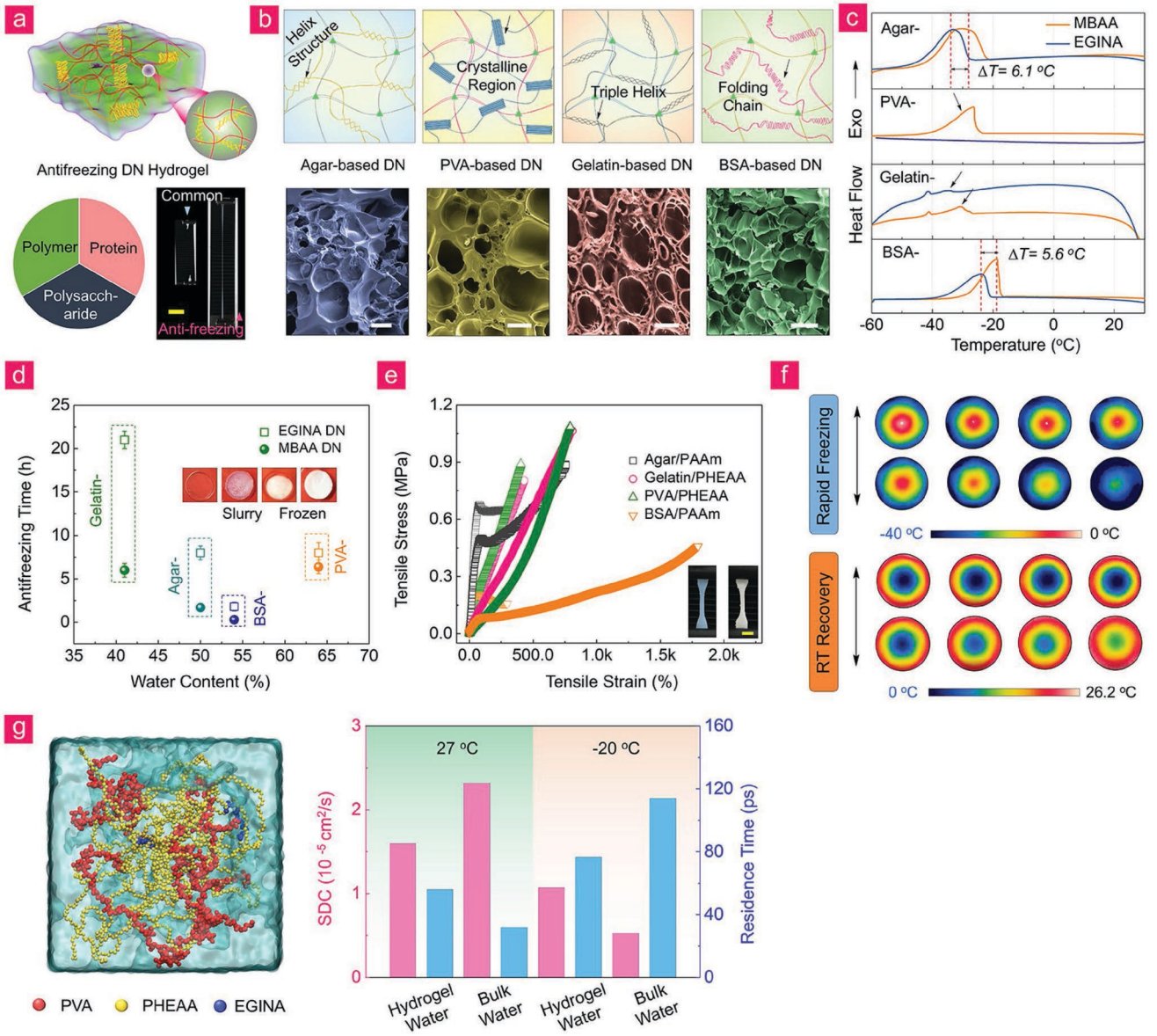

Figure 2. Antifreezing property of EGINA-crosslinked DN hydrogels. a) Design of four types of DN hydrogels of PVA/PHEAA, gelatin/PHEAA, agar/PAAm, and BSA/PAAm hydrogels crosslinked by EGINA. Polymers in these EGINA-crosslinked DN hydrogels are varied from polysaccharides of agar, global protein of BSA and gelatin, and polymer of PVA as the first network to hydrophilic PHEAA and PAAm as the second network. EGINA-crosslinked DN hydrogels exhibit the higher stretchability than MBAA-crosslinked DN hydrogels at frozen states (Scale bar: 5 cm). b) Schematic and SEM images of network organizations and porous structures of (Scale bar: 100 µm). Side-by-side comparison of c) DSC curves and d) antifreezing time as a function of water contents between both EGINA- and MBAA-crosslinked DN hydrogels. Insets in (d) show the appearances of slurry EGINA-crosslinked and frozen MBAA-crosslinked DN hydrogels. e) Uniaxial tensile stress–strain profiles of EGINA-based DN hydrogels (solid curves) in comparison with MBAA-based hydrogels (curves with dim colors) frozen at −20 °C. f) Time-lapse IR images to characterize the temperature distribution of EGINA- and MBAA-crosslinked gelatin/PHEAA DN hydrogels when switching between freezing and warming processes. g) MD simulations of EGINA-crosslinked PVA/PHEAA DN hydrogels, with structural and dynamical characterization (self-diffusion coefficient and residence time) of water molecules in hydrogels as compared to those of bulk water at −20 and 27 °C.

≈200–1000%. The EGINA concentration-dependent mechanical stress–strain curves of agar/PAAm, gelatin/PHEAA, PVA/PHEAA, and BSA/PAAm DN hydrogels at uniaxial elongation processes in Figure S9, Supporting Information also suggested that 5 mol% is an optimal concentration to achieve the superior mechanical strength and stretchability. Despite distinct composition-dependent porous structures due to different polymer conformations and entanglements (Figure 2b), the higher crosslinking densities generally produced the smaller pore sizes. We further prepared eight typical EGINA- and MBAA-crosslinked double-network hydrogels of agar/PAAm, gelatin/pHEAA, BSA/PAAm, and PVA/pHEAA, each representing agar-based, gelatin-based, BSA-based, and PVA-based categories. All of EGINA-crosslinked hydrogels exhibited the faster swelling rates than MBAA-crosslinked hydrogels, implying the stronger water accommodation of EGINA-crosslinked hydrogels (Figure S10, Supporting Information). We applied five successive loading–unloading cycles to assess the self-recovery property of four typical EGINA-crosslinked DN hydrogels with 5 min waiting time between cyclic loadings at room temperature. Collective data in Figure S11, supporting Information showed that i) agar/PAAm and BSA/PAAm DN hydrogels showed obvious stress yielding at low tensile strains, an indicator of strong double-network behavior, while still retaining the toughness/stiffness recovery of 16%/35% for agar/PAAm gels and 50%/48% for BSA/PAAm gels. The recovery process may also be related to the competition between the elasticity of the main network and the strength of the temporarily reformed bonds during the unloading process.[21] ii) For agar/PAAm hydrogel, since the first agar network was so brittle and cannot be recovered by 5 min of resting without heating, both toughness (energy loss) and stiffness (elastic modulus) recovery ratios were largely decreased to 16% and 35% after the first loading–unloading cycle, but remained almost unchanged after the second loading–unloading cycles. iii) Gelatin/PHEAA and PVA/PHEAA hydrogels showed typical elastic properties, as evidenced by stable toughness/stiffness recovery of 82%/98% for gelatin/PHEAA gels and 41%/58% for PVA/PHEAA gels. Obviously, these DN hydrogels showed permanent residual strain due to the damage of the first brittle network at large deformation. Furthermore, we conducted shear rheology tests on EGINA-crosslinked agar/PAAm, BSA/PAAm, PVA/PHEAA, and gelatin/PHEAA DN hydrogels at room temperature by a HAAKE MARS modular advanced rheometer (Thermo Scientific) (Figure S12a, Supporting Information). Four DN hydrogels displayed typical gel-like viscoelastic behaviors,[22,23] where elastic modulus (G') was not only almost independent of frequency, but also an order of magnitude greater than viscous modulus (G''), indicating a predominantly elastic behavior in the frequency range of ≈0.1–100 Hz. It can be clearly observed that four typical DN hydrogels displayed the highly elastic mechanical behavior, as evidenced by the almost linear scaling of $\eta^* \sim \omega$ (Figure S12b, Supporting Information). The resultant scaling exponents of four hydrogels was −0.84, −0.78, −0.74, and −0.68, respectively, all of which were less than a threshold value of −0.98 for fully chemically crosslinked hydrogels.[22] This result indeed confirms the hybrid networks of the four DN hydrogels, that is, the four DN hydrogels consist of the first physically crosslinked network (e.g., agar, BSA, PVA, and gelatin) and the second chemically crosslinked network (e.g., PAAm and PHEAA). DSC results revealed the differences in enthalpy changes between EGINA- and MBAA-crosslinked DN hydrogels during the cooling process from 30 to −60 °C. It can be seen that EGINA-crosslinked agar/PAAm, gelatin/PHEAA, and BSA/PAAm hydrogels exhibited significant exothermic hysteresis, as evidenced by temperature lags by ≈6.1, 4.2, and ≈5.6 °C, while EGINA-crosslinked PVA/PHEAA hydrogels did not shown any heat release peak in sharp contrast to MBAA-crosslinked ones. The disappearance of a freezing point indicates the prevention of free water molecules from the formation of ice crystallization by EGINA in PVA/PHEAA networks (Figure 2c). We further quantified the antifreezing time of eight crosslinked DN hydrogels as a function of water content (Figure 2d and Figure S13, Supporting Information). Independent of network compositions, all of EGINA-crosslinked DN hydrogels took the longer time to achieve a completely frozen state from an as-prepared (i.e., slurry) state than MBAA-crosslinked hydrogels. Such an antifreezing property became more pronounced for EGINA-crosslinked gelatin/PHEAA and agar/PAAm hydrogels. Gelatin/PHEAA@EGINA hydrogel remained its unfrozen, slurry state for 24 h at −20 °C, as compared to 5.5 h to achieve its frozen state for gelatin/PHEAA@MBAA hydrogel. Similarly, agar/PAAm@EGINA hydrogels (≈8.5 h) exhibited the eight times longer antifreezing times than agar/PAAm@MBAA (≈1 h). Moreover, for the same hydrogel systems, the less water contents favored the longer antifreezing time (Figure S13, Supporting Information). On the other hand, among different DN hydrogels, PVA/PHEAA hydrogels containing the highest water content of ≈64% can still retain their slurry state for ≈6 h, which was much longer than other three DN hydrogels, probably because PVA polymers could form high crystallization regions to trap water molecules from aggregation at subzero temperatures.

We next quantified the mechanical properties of EGINA- and MBAA-crosslinked DN hydrogels at −20 °C using tensile, compression, and tearing tests (Figure 2e and Figure S14, Supporting Information). After placing hydrogels at −20 °C for the same time, EGINA-crosslinked DN hydrogels remained soft and deformable to be stretched and bended repeatedly, while MBAA-crosslinked DN hydrogels became too rigid and brittle to sustain any mechanical deformation. Quantitatively, EGINA-crosslinked agar/PAAm, gelatin/PHEAA, PVA/PHEAA, and BSA/PAAm gels exhibited tensile stress/strain of 0.88 MPa/760%, 1.06 MPa/810%, 1.08 MPa/792%, and 0.46 MPa/1795%, all of which were higher than those of the corresponding MBAA-crosslinked DN hydrogels. Similarly, EGINA-crosslinked DN hydrogels (4.6–8.0 MPa, 2650–9400 J m^{-2}) demonstrated the higher compressive stresses and tearing energies than MBAA-crosslinked DN hydrogels (0.81–2.56 MPa, 1200–6400 J m^{-2}) at similar break strains (Figure S14, Supporting Information). EGINA-enhanced mechanical properties, particularly stretchability, are likely stemmed from their non-frozen polymer elasticity, in contrast to the frozen-induced rigid, brittle networks in MBAA-crosslinked hydrogels. Ice crystals formed at subzero temperature stiffen crosslinked polymeric gels, while still allowing certain degree of deformation to occur, similar to the toughening of nanocomposite hydrogels. 2D-FTIR synchronous and asynchronous spectra revealed that a temperature-dependent band

at ≈3100–3400 cm^{-1} assigning to hydroxy (-OH) stretching underwent a significant change for MBAA-crosslinked hydrogels, while this band was almost unchanged for EGINA-crosslinked hydrogels (Figure S15, Supporting Information). Band changes in MBAA-crosslinked hydrogels indicate the dramatic disruption of hydrogen bonds between hydroxy/amino (BSA/PAAm) groups and hydroxyl (water) groups. Time-lapse IR images further revealed the in situ temperature distribution of EGINA- and MBAA- crosslinked hydrogels when switching between −60 °C (freezing) and 26.2 °C (warming) temperatures. In Figure 2f, during the freezing process from −60 to 0 °C, EGINA-crosslinked hydrogels remained their original temperature distribution almost unchanged as time, showing a highly freezing-resistant property, in sharp contrast to a fast melting process of MBAA-crosslinked hydrogels (Figure S16 and Videos S4 and S5, Supporting Information). Similar temperature distributions were observed for EGINA- and MBAA-crosslinked hydrogels during the warming process from 0 to 26.2 °C. This also implies that the relatively steady temperature gradients in EGINA-crosslinked DN hydrogels impose additional free energy barriers for ice nucleation. More importantly, we conceptually constructed phase diagrams of these four EGINA-crosslinked DN hydrogels by collecting all available experimental data (Figure S17, Supporting Information). All hydrogels displayed similar ternary phase diagrams, in which the increase of gel network contents indicates the less water content, thus resulting in the lower freezing points of hydrogels, which in turn defines a slurry region to separate hydrogel and frozen regions from each other. Taken together, the integration of strong water-binding EGINA crosslinkers and polymers with tightly crosslinked and highly interpenetrating DN structures allows to impose both strong compositional and spatial effects to enhance polymer–water interactions for competitively depressing ice nucleation, accumulation, and growth. Thus, EGINA plays a decisive role in reducing the freezing point of all tested DN hydrogels, independent of their network compositions. We computationally constructed EGINA-crosslinked PVA/PHEAA DN hydrogels (Figure 2g), followed by the all-atom MD simulations to characterize the structure, dynamics, and interactions of water molecules confined in hydrogels at 27 and −20 °C. RDFs of water molecules in hydrogels at both temperatures showed almost identical distributions, which were similar to that of bulk water, but differ from that of bulk ice (Figure S18, Supporting Information). Dynamically, hydrogel water exhibited the higher self-diffusion coefficients and the shorter residence time (Ct) than bulk water (ice) at −20 °C, showing a liquid-like behavior. But, this trend became opposite at 27 °C, that is, hydrogel water is less mobile than bulk water at 27 °C due to spacious confinement effect (Figure 2g and Figure S18, Supporting Information). Collectively, simulation results suggest that confined waters in polymer network tend to maintain their unfrozen and liquid-like structures and dynamics.

2.3. Optimization of EGINA-crosslinked Antifreezing Hydrogels by the Secondary Networks

To further examine our crosslinker-driven antifreezing strategy capable for expanding to other DN hydrogel systems, we designed and polymerized four types of monomers including zwitterions (SBAA, VBPS, SBMA, and SVBA), electrolytes (DMAE, AAc, AMPS, and META), hydrophilies (AAm, HEAA, HEMA, and HEA), macromolecules (PEGDA and GelMA) to construct distinct second network interpenetrating with the first protein/polymer/polysaccharide network (**Figure 3**a and Table S2, Supporting Information), producing a total of 28 EGINA- and MBAA-crosslinked DN hydrogels. The as-synthesized monomeric structures were characterized and confirmed by ^{1}H-NMR (Figures S19–S21, Supporting Information). Mechanical properties of these different EGINA- and MBAA-crosslinked DN hydrogels at −20 °C were summarized in Figure 3b and Figure S22, Supporting Information. At room temperature, DN hydrogels formed by the second, hydrophilic network (green area) possessed the higher tensile properties than other DN hydrogels, while DN hydrogels with zwitterionic and macromolecule networks (brown area) were too weak to sustain the large mechanical deformation. Such mechanical differences among these hydrogels were closely related to their antifreezing capacities. Specifically, EGINA and hydrophilic network can synergistically form a variety of molecular clusters with water molecules at the expense of hydrogen bonds between water molecules, therefore significantly reducing freezing point and maintaining mechanical properties at gel-like state. Differently, zwitterionic networks may over-crosslink with water molecules via ionic interactions, while macromolecule networks have insufficient binding sites to form hydrogen bonds with water molecules due to their well-folded structures. Both scenarios prevent water molecules from ice nucleation, thus leading to mechanically brittle and rigid hydrogels at subzero temperatures. The antifreezing-induced mechanical properties of hydrogels containing electrolyte networks behaved in between hydrophilic and zwitterionic/macromolecule network containing hydrogels.

Further comparison of freezing tolerance between EGINA- and MBAA-crosslinked hydrogels exhibited strong the network composition-dependent antifreezing performance (Figure 3c). Specifically, gelatin/zwitterions and gelatin/electrolytes hydrogels presented the longer antifreezing time of 16–21 h at −20 °C. These hydrogels contain a large number of charge groups (e.g., sulfobetaine, quaternary ammonium ion, dimethylamine oxide, and dimethyl sulfoniopropionate), which are well known to have strong binding with water via salt/ionic-induced solvation. Thus, antifreezing property of these hydrogels often comes from their associated ions (salts) in solution to depress the freezing points of water, showing similar ion-induced antifreezing mechanism to salt-additive hydrogels. More interestingly, zwitterionic polymers often exhibit "anti-polyelectrolyte effect" behavior, that is, they adopt a fully stretched chain conformation in salt solution, but a collapsed chain conformation in water. This anti-polyelectrolyte behavior is completely opposite to polyelectrolyte materials. But, both types of hydrogels still exhibited similar antifreezing properties, further confirming the ion-induced antifreezing mechanism. Differently, EGINA-crosslinked gelatin/hydrophilic hydrogels can greatly extend antifreezing time to 24 h, as compared to MBAA-crosslinked hydrogels (≈9 h). Hydrophilic polymers resemble alcohol-like amphiphilic structures, whose hydrophilic amide, hydroxyl, carbonyl groups allow to form hydrogen bonds with water molecules by reducing the number of free water molecules that

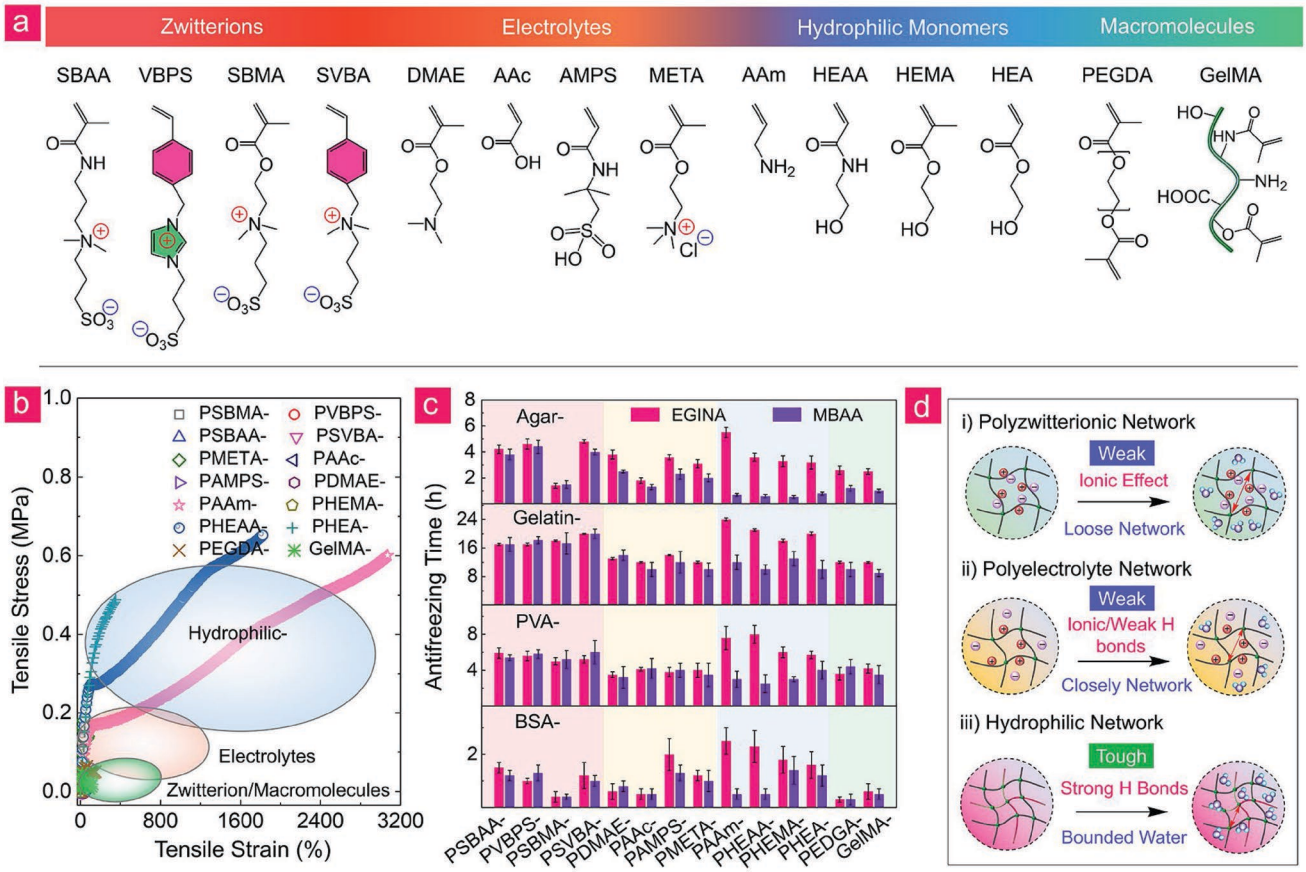

Figure 3. Exploration and optimization of EGINA-crosslinked antifreezing hydrogels by the secondary networks. a) Four types of monomers of zwitterions (i.e., SBAA, VBPS, SBMA, and SVBA), electrolytes (i.e., DMAE, AAc, AMPS, and META), hydrophilies (i.e., AAm, HEAA, HEMA, and HEA), and macromolecules (i.e., PEGDA and GelMA) used for constructing the second network and examining their composition effects on antifreezing and mechanical properties of the resultant DN hydrogels. b) Tensile stress–strain curves of agar-based DN hydrogels with different secondary networks from (a) at –20 °C. c) Summary and comparison of antifreezing time among agar-based (50 wt%), gelatin-based (43 wt%), PVA-based (64 wt%), and BSA-based (54 wt%) DN hydrogels crosslinked by EGINA and MBAA and formed by four types of the second networks from (a). d) Schematic illustration of the role of the secondary network in network interactions and structures in relation to their antifreezing and mechanical properties of EGINA-crosslinked DN hydrogels.

help to lower the freezing point, while their hydrophobic backbones tend to aggregate to form crystalline domains that give rise of high mechanical strengths of the hydrogels (Figure 3d). Macromolecules as the second networks involved more complex interactions with water molecules and the first networks, strongly depending on their specific folding structures. In general, EGINA and hydrophilic polymer chains synergistically lock water molecules, which in turn competitively disrupts the hydrogen-bonded aggregation of free water molecules, thus leading to the decrease of water freezing points (lower the vapor pressure of water) and the activation of multiple energy dissipation pathways of water–network, network–network, and water–water interaction for enhancing the mechanical properties of hydrogels at subzero temperatures.

2.4. Applications of Antifreezing Hydrogels as Smart Devices at Subzero Temperatures

Different from most of the antifreezing hydrogels being used as strain sensors or conductors, we applied our antifreezing EGINA-crosslinked gelatin/PHEAA hydrogels for smart windows with a sandwich structure consisting of an antifreezing hydrogel layer in between the two glasses (**Figure 4**a). This sandwich design allows to prevent volume changes caused by water–ice phase transition and transparency issue caused by the loss of water.[24] Evidently at 25 °C, the sandwiched gelatin/PHEAA hydrogels can effectively prevent moisture evaporation and thus retain ≈99% of water in hydrogels for 100 h, in sharp contrast to a significant water loss (48%) of pure gelatin/PHEAA hydrogel (Figure 4b). Next, we compared the optimal transmittance variations of both EGINA- and MBAA-crosslinked gelatin/PHEAA hydrogel windows at a light wavelength range from 350 to 1100 nm (Figure 4c) and at a specific light wavelength of 800 nm (Figure 4d). EGINA-crosslinked gelatin/PHEAA hydrogel windows can still retain 50% of optical transmittance at –20 °C for 2 h as compared to 90% at room temperature, but MBAA-crosslinked hydrogel windows became completely opaque with 0% of optical transmittance at the same frozen conditions (Figure 4c and Video S6, Supporting Information). Consistently, Figure 4d also showed that at a NIR wavelength of 800 nm, EGINA-crosslinked hydrogel windows

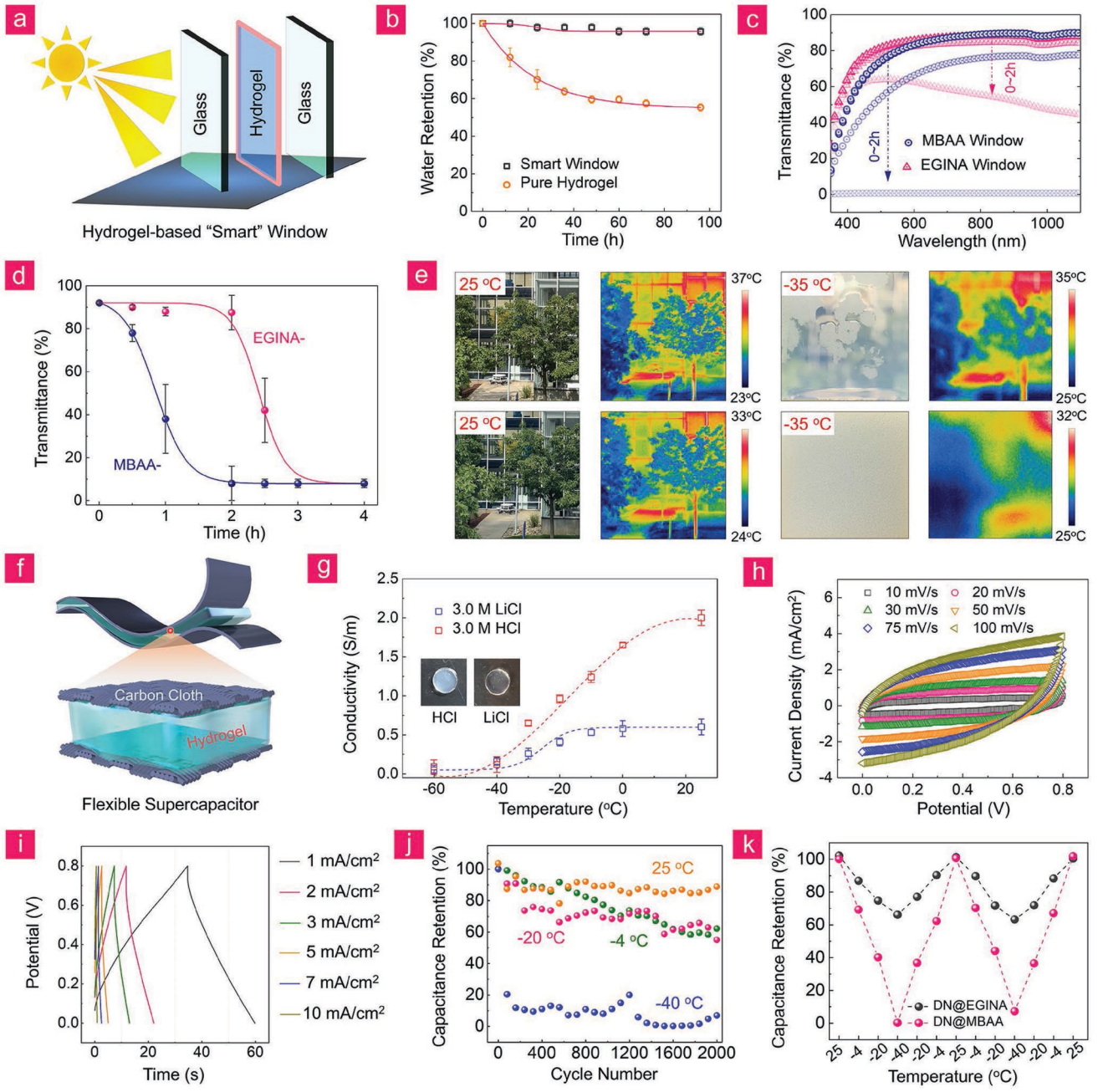

Figure 4. Applications of antifreezing hydrogels to different devices. a) Schematic design of a sandwiched antifreezing hydrogel window. b) Time-dependent water retention of pure gelatin/PHEAA hydrogel and sandwiched gelatin/PHEAA hydrogel window at humidity/temperature of 28%/25 °C. c) Optical transmittance of EGINA- and MBAA-crosslinked gelatin/PHEAA hydrogel windows at UV–Vis wavelengths of 350–1100 nm at –20 °C. d) Time-dependent optical transmittance of EGINA- and MBAA-crosslinked gelatin/PHEAA hydrogel windows at 800 nm wavelength and –20 °C. e) Side-by-side comparison for optical transparency and temperature distribution between EGINA-crosslinked gelatin/PHEAA and PNIPAM hydrogel windows at –35 and 25 °C. f) Schematic design of antifreezing hydrogel-based supercapacitors (ACC//hydrogel electrolytes//ACC) with a sandwiched structure. g) Conductivity of HCl or LiCl-doped PVA/PHEAA@EGINA hydrogel electrolytes as a function of temperature (≈–60–25 °C). h) CV and i) GCD curves of PVA/PHEAA@EGINA supercapacitors at different scanning rates (≈10–100 mV s^{-1}) and current densities (≈1–10 mA cm^{-2}) at –20 °C. j) Capacity retention of PVA/PHEAA@EGINA supercapacitors at different temperatures from –40 to 25 °C upon 2000 cycles. k) Reversibility of capacity retention for PVA/PHEAA@EGINA and PVA/PHEAA@MBAA supercapacitors during reversible cooling and heating processes between 25, –4, –20, and –40 °C.

exhibited a significant delay of transmittance reduction from 90% to 0% at –20 °C for 4 h, in sharp contrast to a rapid transmittance reduction to 0% (2 h) in pure HEMA hydrogel. The increase of transparency in EGINA-crosslinked hybrid windows is likely attributed to the enhanced non-frozen water content by EGINA and polymer networks, because they will strongly bind to a large amount of water molecules at the expense of ice crystals formed by free water molecules inside hydrogels, which in

turn reduces the scattering centers and leads to the better gel transparency. Different from current PNIAPM hydrogel-based smart windows,[25] they often suffer from poor transparency caused by the frozen-induced scattering center effect at subzero temperatures, that is, the higher ice crystals will lead more light to be scattered at the water–polymer interface, resulting in lower light transmission in visible wavelengths. More importantly, the gelatin network exhibits a thermo-reversible sol–gel transition, that is, upon cooling the gel from melting temperatures of 26–30 °C, gelatin undergoes a structural transition from coils at a sol state to helices at a gel state. Such temperature-induced reversible structural transition allows the gelatin-based smart windows to adsorb or release energy as temperature changes from 26 to 30 °C. Evidently, thermal IR images of EGINA-based hydrogel windows clearly showed the heterogeneous temperature distributions, which reflect not only different optical transmittance outside temperatures, but also the shapes of objectives (e.g., tree, ground, and building) outside window (Goodyear Polymer Center, Ohio). Conversely, PNIPAM-based hydrogel window completely lost its optical transmittance and temperature distribution due to heterogeneous ice crystals (−35 °C) (Figure 4e).

Next, to address an issue of conventional conductive hydrogels that will freeze and lose their conductivity at subzero temperatures, we fabricated sandwiched supercapacitors consisting of two carbon cloth layers and an antifreezing EGINA-crosslinked PVA/PHEAA hydrogel electrolytes (Figure 4f). To further enhance electrical conductivity and stability, the hydrogels were pretreated with the electrolyte solutions of 3.0 M HCl or LiCl. For comparison, LiCl-doped hydrogel electrolytes enabled to maintain the conductivity of ≈0.5 S m^{-1} even under −20 °C, while HCl-doped hydrogel electrolytes lost almost 50% of conductivity (Figure 4g and Figure S23, Supporting Information). After the device assembly by PVA/PHEAA@EGINA hydrogels, electrochemical CV profiles in Figure 4h and Figure S24, Supporting Information showed that all of charge–discharge CV curves displayed typical parallelogram shapes at both 25 and −20 °C, an indicator of electrostatic double-layer capacitors (EDLC) characteristics, whose areas increased as scanning rates (10–100 mV s^{-1}). Consistently, electrochemical kinetics and ionic resistance of PVA/PHEAA@EGINA devices remained almost unchanged at −20 °C. The high conductivity of PVA/PHEAA@EGINA devices under subzero temperatures is mainly attributed to a combination of antifreezing property, LiCl incorporation, and polymer–water binary network, all of which allows to facilitate ion migration and electrical percolation pathways. Further, we built an in-house cooling system to challenge the cold tolerance to the charge–discharge stability of our hydrogel supercapacitors. Galvanostatic charge–discharge curves at different current densities in Figure 4i showed that the maximum specific capacitance of PVA/PHEAA@EGINA electrolytes was ≈16–45 mF cm^{-2} at a current density of ≈10–100 mA cm^{-2} under −20 °C, while the Coulombic efficiencies of the AF battery remained as high as approximately 100% even at −20 °C.

PVA/PHEAA@EGINA supercapacitors delivered a capacity of 20 mF cm^{-2} (5 mA cm^{-2}) with a retention of ≈87% of its initial capacity after 2000 cycles at 25 °C (Figure 4j). A cycling stability of the supercapacitors was also manifested as evidenced by 60.2% at −4 °C and 56.3% at −20 °C of capacity retention over 2000 cycles. Further decrease of temperature to −40 °C caused a significant drop of capacity retention to ≈10% after 100 cycles. In Figure 4k, PVA/PHEAA@EGINA supercapacitors delivered a capacity of 20 mF cm^{-2} (≈99% of capacitance retention) at 25 °C, 23 mF cm^{-2} (89.3% of capacitance retention) at −4 °C, 16 mF cm^{-2} (74.8% of capacitance retention) at −20 °C, and 8.1 mF cm^{-2} (68.3% of capacitance retention) at −40 °C, showing a temperature-dependent capacity retention behavior. While electronic capacity decreased as temperatures, it can be completely recovered to original values as temperature increased from −40 to 25 °C. No significant capacity loss was observed after four cycles between cooling and heating processes. For comparison, MBAA-crosslinked PVA/PHEAA electrolytes underwent a significant loss of capacitance retention from 67.3% at −4 °C, 31.8% at −20 °C, to ≈7.9% at −40 °C (Figure 4k). The cycling results confirm the importance of EGINA antifreezing property for achieving high and stable electronic capacity and conductivity at subzero temperatures.

3. Conclusions

We demonstrated a simple, crosslinker strategy to design a new family of EGINA-crosslinked DN hydrogels made of a wide variety of network compositions, including zwitterions, electrolytes, hydrophilies, and macromolecules. All of the resultant DN hydrogels containing ≈43–90 wt% water exhibited an intrinsic antifreezing property at subzero temperatures. Since EGINA-crosslinked DN hydrogels were free of any antifreezing additives, which were fundamentally different from the existing antifreezing hydrogels with antifreezing additives, the antifreezing mechanism is solely derived from the formation of tightly bound water with networks via hydrogen bonds and the confinement of the water in tightly crosslinked DN structures, almost independent of their network compositions. Benefiting from excellent freezing resistance and mechanical properties, EGINA-crosslinked DN hydrogels can be further fabricated into smart windows with high optical transmittance and supercapacitors with excellent electrochemical stability at subzero temperatures. Hydrogel-based windows allowed to retain high transparency, temperature sensitivity, and frozen-induced volume expansion at −20 °C over 24 h, while hydrogel-based supercapacitors not only enabled a 60% capacity retention at −20 °C after 2000 cycles, but also retained almost 100% capacity retention during multiple cooling and heating processes between −40 and 25 °C. This work demonstrates a new, simple crosslinker strategy to fabricate a wide variety of DN hydrogels and hydrogel-based devices with freezing tolerance and robust mechanics, in which antifreezing design principle and antifreezing hydrogel systems will offer new insights into the design of next-generation antifreezing materials/coatings without any additives beyond few available today.

4. Experimental Section

Materials: Monomers, including *N*-(3-sulfopropyl)-*N*-methacryloylamidopropyl-*N*,*N*-dimethylammonium betaine (SBAA,

97%), 2-(methacryloyloxy) ethyl]dimethyl-(3-sulfopropyl) ammonium hydroxide (SBMA, 98%), 2-(dimethylamino)ethyl methacrylate (DMAE, 98%), acrylic acid (AAc, 98%), 2-acrylamido-2-methylpropane-1-sulfonic acid (AMPS, 98%), [2-(methacryloyloxy)ethyl]-trimethylammonium chloride (META, 75wt%), acrylamide (AAm, 98%), *N*-hydroxyethyl acrylamide (HEAA, >98%),2-hydroxyethyl methacrylate (HEMA, 97%), 2-hydroxyethyl acrylate (HEA, 98%), poly(ethylene glycol) diacrylate (PEGDA, 98%, M_w = ≈700 g mol^{-1}), polyvinyl alcohol powder (PVA, M_n = 140 000 g mol^{-1}), agar (gel strength >300 g·cm^{-2}, and melting point 85–95 °C), gelatin (type A, gel strength ≈300 g·cm^{-2}), 2-hydroxy-4′-(2-hydroxyethoxy)-2-methylpropiophenone (Irgacure 2959, 99%), and MBAA (98%) were received from Sigma-Aldrich Inc. Some other uncommercial monomers were synthesized and characterized in the Supporting Information. Water used in these experiments was purified by a Millipore water purification system with a minimum resistivity of 18.0 MΩ cm. All other reagents were commercially obtained and used as received without any purification.

Synthesis of EGINA: The crosslinker EGINA was synthesized via additive reaction by coupling 2-isocyanatoethyl acrylate and glycol. Generally, after degassed by nitrogen flow, 2-isocyanatoethyl acrylate (5 g, 0.035 mol) was added dropwise to the 25 mL flask containing glycol (1.055 g, 0.017 mol) under continuous stirring at 0 °C for 3.0 h. The reaction between isocyanate and hydroxyl groups was a fully additive reaction, which means no by-products would be generated. The resulting EGINA liquid was then stored in the −20 °C freezer.

Fabrication of Binary Polymer–Water Hydrogels: All binary polymer–water hydrogels were mainly synthesized according to the previous literatures. Particularly, DN hydrogels consisted of first physical-crosslinked network and secondary chemical-crosslinked network. Several monomers were selected as to form secondary chemical-crosslinked networks, including zwitterions (SBAA, SBMA, VBIPS, and SVBA), electrolytes (DMAE, AAc, AMPS, and META), hydrophilic monomers (AAm, HEAA, HEMA, and HEA), and macromolecules (PEGDA and GelMA). The schematic for photopolymerization process and detailed discussion are provided in Figures S1 and S2, Supporting Information.

Typically, agar-based hydrogels were synthesized by following our previous work via a one-pot method.[26] For example, agar (100 mg), AAm (1.0 g), Irgacure 2959 (1 mol% of monomer), crosslinker (MBAA/EGINA, 0.1/5 mol% of monomer) and water (≈2.0–5.0 mL) were added into a tube. After several degassing cycles, the tube was sealed under high-purity nitrogen and heated at 90 °C in an oil bath. After the mixtures became transparent (≈10 min), the hydrogel precursors were immediately injected into prearranged glass molds and then cool down at room temperature for 2.0 h (thickness: 1 mm). Once the first physical network (agar) formed, the gel molds were exposed under UV irradiation (UVL-28, 8 W, ≈800 µW cm^{-2}) for 1.5 h to achieve >90% of gel fraction.

For gelatin-based hydrogels, a typical mixture containing gelatin (0.7 g), HEAA (3.0 g), I-2959 (1 mol%), crosslinker (MBAA/EGINA, 0.1/5 mol% of monomer), and water (≈3.0–6.0 mL) was added into a reactor. The solution was degassed and fully dissolved after heating at 65 °C for ≈10 min. The transparent precursor was then immediately injected into a sealed glass mold with a 1.0 mm thickness and placed it at 4 °C for 4.0 h to form physical gelatin networks. Once the first physical network formed, the glass mold was exposed under UV irradiation (UVL-28, 8 W, ≈800 µW cm^{-2}) for 1.5 h to achieve >90% of gel fraction.

BSA-based hydrogels were also synthesized by the modified one-pot method. For instance, BSA (≈0.29–0.5 g mL^{-1}), AAm (1.2 g), Irgacure 2959 (1 mol% of AAm), and crosslinker (0.1/5 mol% of AAm) were dissolved into H_2O (4.0 mL) in a reactor. After degassing three times, the reactor was sealed under high-purity N_2 atmosphere. The reactants were fully dissolved and subsequently injected into a plastic mold with the thickness of 1 mm, followed by a heating procedure at 80 °C for 10 min to form the BSA network in an oven. Once the first physical networks formed, the gel molds were then exposed under UV irradiation (UVL-28, 8 W, ≈800 µW cm^{-2}) for 1.0 h to achieve >90% of gel fraction.

As for PVA-based hydrogels, 3.0 g prepared PVA solution (10 wt%), HEAA (≈0.3–1.2 g), Irgacure 2959 (1 mol% of monomer), crosslinker (MBAA or EGINA, 0.1/5 mol% monomer) were fully dissolved in a small beaker at 60 °C for 5 min. Subsequently, the transparent solution was injected into a glass mold separated by 1 mm thickness of poly(tetrafluoroethylene) (PTFE) and put into −80 °C refrigerator for 4 h. The frozen gel then thawed under the room temperature for another 4 h. After three freeze-thawing cycles, the PVA networks would be formed. Subsequently, the prepared hydrogels soon exposed under UV irradiation (UVL-28, 8 W, ≈800 µW cm^{-2}) for another 1.0 h, to form the secondary networks with >90% of gel fraction.

The above-mentioned protocols for some peculiar systems are optimized, for more detailed information please see Table S2, Supporting Information.

Molecular Simulation of Crosslinkers and Polymer Solutions: Atomic volume of MBAA and EGINA aqueous solution and their polymer solutions (Case 1 (-$PAAM_{20}$-), and Case 2 (-$PAAM_{10}$-)) were simulated using LAMMPS with CHARMM force field. The pre-prepared polymer chains for were put into a 6 nm × 6 nm × 6 nm water box, and relaxed for 10^{-10} s after a conjugate gradient (CG) algorithm minimization with a time step of 10^{-15} s using isothermal–isobaric (NPT) ensemble at 1 atmosphere and 280 K. Then temperature reduced to 160 K with a cooling rate of 3×10^9 K s^{-1}, and the whole system for both of the cases underwent equilibrium for 5×10^{-10} s.

Modeling of PVA/PHEAA DN Hydrogel and Simulation Protocol: In this work, a computational "random walk reactive polymerization" (RWRP) algorithm[27] to construct the PVA/PHEAA DN hydrogels was also developed. PVA/PHEAA DN hydrogel with the water content of 50 wt% since it was experimentally demonstrated the optimal antifreezing capacity was constructed. The initial PVA/PHEAA DN hydrogel consists of uncrosslinked PVA network and crosslinked PHEAA network. The force fields of PVA, PHEAA, and EGINA were built using CGenFF (https://cgenff.paramchem.org/), which is compatible with CHARMM force field.[28] To mimic experimental condition under which the PVA/PHEAA DN hydrogel can achieve its excellent antifreezing capability to greatly reduce the ice crystallization rate of water molecules at subzero temperature (e.g., −20 °C), the mass ratio of PVA to PHEAA was assumed to be 3:20. Based on the pre-determined PVA/PHEAA ratio of DN hydrogel, the number of polymer segments/polymerization degrees are set as 6/50 for PVA network and 10/75 for PHEAA network. Before polymerization of the DN hydrogel, the coordinates of 300 (6 × 50) monomers of PVA were randomly initiated in a predefined cell. The DN hydrogel was constructed by densely preconstruction of PVA network in a periodic simulation box. Then, PHEAA network was built by mixing 750 (10 × 75) HEAA monomers with the resulting PVA SN network, which allows the PHEAA network to be constructed with polymer chains randomly crossing PVA network through entangling, stretching, bending, and torsion. This computational polymerization process mimics the actual polymerization reaction process of DN hydrogels. For each polymerization step of PVA network and PHEAA network, the polymerization system was optimized using a combination of 5000-step minimizations by conjugate gradient minimization algorithm and 0.02-ns MD simulations in implicit solvent model. From the experimental perspective, hydrogel networks involving crosslinks can inhibit the polymer dissolution into the solvent. For DN hydrogel, two EGINA crosslinkers were added into the resultant DN hydrogels to chemically crosslinked PHEAA chains with four PHEAA segments symmetrically through linking adjacent PHEAA segments. Then, the resulting crosslinked PVA/PHEAA networks were immersed in a cubic box with the dimensions of 56 Å × 56 Å × 56 Å using explicit TIP3P solvent model, which mimic the water content of 50 wt% for the PVA-PHEAA DN hydrogel.

The DN hydrogels with 50 wt% were simulated at two constant temperatures of 253 and 300 K. Initially, the resulting DN hydrogel systems were energy minimized using 5000-step conjugate gradient minimizations to remove bad contacts between atoms and relax the systems. Then, 120-ns all-atom MD simulations carried out using NAMD 2.13 package[29] with CHARMM27 force field under the 3D periodic boundary condition and the NPT ensemble (constant number of atoms, constant pressure, and constant temperature). The temperature was

maintained at 253 or 300 K using the Langevin thermostat method with the damping coefficient of 1 ps^{-1} and the pressure was continuously kept at 1 atm by Langevin Piston with a decay period of 100 fs and a damping time of 50 fs based on the Nose–Hoover algorithm. Long-range electrostatic potentials were calculated by the particle mesh Ewald (PME) method with a grinding space of 1 Å, while short-range VDW potentials were estimated using switch function with twin-range cutoff at 12 and 14 Å, respectively. All covalent bonds of molecules in the systems including hydrogen bonds were constrained using the RATTLE method, hence the velocity Verlet method was conducted to integrate Newton's equations of motion with a larger time step of 2 fs. MD trajectories of all systems were saved every 2 ps for further analysis. All analyses were performed in VMD package[30] using the in-house codes.

Preparation of Antifreezing Hydrogel-Based Smart Devices: Similar to the most common configurations for hydrogel-based smart windows was the sandwich structure, where the adapted antifreezing hydrogel was sandwiched between two pieces of glass sheets. The thickness of the hydrogel layer was controlled by using thermo-plastic sealing films or silicone sheets (1 mm). The typical size of as-prepared smart window was 10×10 cm^2. As for smart hydrogel-based supercapacitors, antifreezing hydrogels conjugated with two pieces of activated carbon cloths to form tight sandwich-type construction. The cells were subsequently immersed into different aqueous supporting electrolytes (3.0 M HCl or LiCl) for ≈10 min, followed by encapsulating with parafilm.

Nuclear Magnetic Resonance Spectra: The chemical structures of synthetic functional monomers were measured on Bruker Avance AMX-400 NMR Spectrometer in D_2O or DMSO-d_6 using tetramethylsilane as an internal reference.

Gel fraction Test: Typically, a gel disk (diameter of 25 mm, thickness of 1 mm) was fully freeze-dried in a freeze-dryer at −70 °C for 24 h. The weight of obtained aerogel was referred as m_0. Afterward, the classical Soxhlet extraction method was applied to the aerogel by immersing it into ethanol (or acetone), followed by a continuous extraction for 24 h. In this way, the uncrosslinked polymers and dissociative monomers are expected to be fully removed from the gel networks, leading to the final weight of m_1. (Note that the residues, i.e., ethanol or acetone will be removed when placed it in the oven at 65 °C for 12 h). The gel fraction (crosslinking efficiency, gel fraction %) can be obtained by the following equation:

$$\text{Gel fraction } \% = \frac{m_1}{m_0} \times 100\% \quad (1)$$

Scanning Electron Microscopy: The morphologies of four kinds of binary polymer–water hydrogels were characterized by scanning electron microscope (SEM, TESCAN).

Laser Scanning Confocal Microscopy: In situ microscopic images were recorded by a laser scanning confocal microscope equipped a time-lapse model. Particularly, the cold stage was home-made, while the temperature range can be controlled from −10 to −60 °C (drikold or liquid nitrogen was applied as freezing media).

Infrared Thermal Imaging: The surface temperature distribution of adopted hydrogels and corresponding IR images were taken by using an infrared thermal imager (TG165, FLIR).

Fourier Transform Infrared Spectroscopy: The fully freeze-dried hydrogel samples were conducted by using a Nicolet-6700 with resolution of 4 cm^{-1} and 32 scans in the range of 4000–600 cm^{-1}, which was further analyzed by 2DShige 1.3 software to obtain 2D images.

UV–Vis Spectra: UV–Vis spectra of solution and hydrogels over the wavelength range of ≈340–1100 nm were recorded by virtue of a UV–Vis spectrophotometer (UV1800, Shimadzu Co., Ltd).

Dynamic Thermal Analysis: Weight loss of solutions and hydrogels were characterized by thermo-gravimetric analysis (TGA, Q500) from 25 to 200 °C at a heating rate of 10 °C min^{-1} under N_2 atmosphere. Differential scanning calorimetry (DSC) was recorded by a Discovery DSC250 (TA Instruments, USA) under N_2 atmosphere. Typically, a small gel disc was encapsulated in a hermetic Aluminum pan and controlled heating rate of 10 °C min^{-1} (Cool–Heat–Cool mode).

Circular Dichroism Spectra: The secondary structure of BSA proteins in EGINA or MBAA aqueous solutions was continuously monitored by a far-UV CD spectropolarimeter (J-1500, Jasco Inc., Japan) equipped with a temperature controller.

Rheological Measurements: Shear viscosity was measured on a HAAKE MARS III rheometer (Thermo Scientific) equipped with a 20 mm parallel plate with shear rates ranging from 0.001 to 50 s^{-1} at room temperature, while the dynamic frequency sweep was conducted from 0.1 to 100 Hz in the oscillatory mode with an optimized oscillatory strain of 1% at room temperature.

Dynamic Mechanical Analysis: For mechanical property measurements, as-prepared hydrogels were cut into dumb-bell shape with a width of 3.18 mm, a gauge length of 25 mm, and a thickness of 1.0 mm. Tensile measurements were all performed on a universal tensile machine (Instron 3345, MA) with a 500 N transducer at the stretching rate of 100 mm·mm^{-1}. Cylindrical hydrogel samples (≈13 mm of height and 9 mm of diameter) were used for compression tests at 20%·min^{-1}. Moreover, the hydrogel sample with trousers shape (40 mm of length, 25 mm of width, and 1 mm of thickness) and an initial notch of 20 mm was applied to tearing test. One arm of the hydrogel sample was clamped and fixed, while another one was clamped and pulled up at a rate of 200 mm·min^{-1}. In order to test mechanical properties of the frozen hydrogels, keep the testing temperature at subzero in advance.

For hysteresis measurement, hydrogels were first stretched to an extension ratio and then unloaded. After returning to the original length, the specimens were reloaded and stretched to the same extension ratio (300% or 400%) at 100 mm min^{-1}. This loading–unloading cycle was repeated five times. Here, dissipated energy was estimated by area below the stress–strain curves or between the loading–unloading curves. As for successive loading–unloading cyclic measurements, the operations were repeatedly conducted on the same specimen with increasing extension ratios (λ = 200%, 400%, 600%, and 800%) until the sample failed at an elongation break.

Electrochemical Measurements: The electrochemical characteristics, that is, cyclic voltammetry (CV; ≈10–100 mV s^{-1}), galvanostatic charge–discharge (GCD, ≈1–10 mA cm^{-2}), and electrochemical impedance spectrum (EIS) of hydrogel-based supercapacitors were tested by a Gamry Reference 3000 electrochemical workstation (Gamry Instruments, USA). Typically, EIS measurements were performed at the frequency range of ≈10 mHz to ≈100 kHz, while the impedance amplitude was ±5 mV at open circuit potential. Conductivity of tested hydrogel electrolytes (2×2 cm^2) was firstly measured by four-probe AC impedance spectrum at the temperature range of ≈−60–25 °C.

Supporting Information

Supporting Information is available from the Wiley Online Library or from the author.

Acknowledgements

J.Z. thanks financial support from NSF (1825122 and 1806138) and Faculty Summer Fellowship from University of Akron. Y.P. and L.X. thank financial support from NSF (1824840). The authors also thank three K12 students of Keven Gong from Hudson Middle School, Alice Xu from Hudson High School, and Bowen Zheng from Copley High School for grammatical checking and correction.

Conflict of Interest

The authors declare no conflict of interest.

Author Contributions

J.Z. supervised this project. J.Z. and D.Z. conceived the concepts and designed the research. D.Z. synthesized and characterized EGINA, uncommercial functional monomers, and hydrogels. Y.L., Y.P., L.X. conducted computational modeling and simulations of polymers and hydrogels. D.Z., Y.L., and X.G. conducted electrochemical experiments for hydrogel-based supercapacitors. D.Z. and J.Z. mainly wrote the manuscript. All authors participated in the discussion of the results.

Data Availability Statement

Research data are not shared.

Keywords

antifreezing, crosslinkers, hydrogels, smart devices

Received: May 26, 2021
Revised: July 22, 2021
Published online: September 2, 2021

[1] Z. He, C. Wu, M. Hua, S. Wu, D. Wu, X. Zhu, J. Wang, X. He, *Matter* **2020**, *2*, 723.

[2] a) S. Jung, M. K. Tiwari, D. Poulikakos, *Proc. Natl. Acad. Sci. U. S. A.* **2012**, *109*, 16073; b) S. W. Wu, Z. Y. He, J. Zang, S. L. Jin, Z. W. Wang, J. P. Wang, Y. F. Yao, J. J. Wang, *Sci. Adv.* **2019**, *5*, eaax3793.

[3] a) P. M. Naullage, V. Molinero, *J. Am. Chem. Soc.* **2020**, *142*, 4356; b) J. Chen, J. Liu, M. He, K. Li, D. Cui, Q. Zhang, X. Zeng, Y. Zhang, J. Wang, Y. Song, *Appl. Phys. Lett.* **2012**, *101*, 111603; c) Z. He, K. Liu, J. Wang, *Acc. Chem. Res.* **2018**, *51*, 1082.

[4] S. Wu, Y. Du, Y. Alsaid, D. Wu, M. Hua, Y. Yan, B. Yao, Y. Ma, X. Zhu, X. He, *Proc. Natl. Acad. Sci. U. S. A.* **2020**, *117*, 11240.

[5] K. Golovin, A. Tuteja, *Sci. Adv.* **2017**, *3*, e1701617.

[6] H. Gao, Z. Zhao, Y. Cai, J. Zhou, W. Hua, L. Chen, L. Wang, J. Zhang, D. Han, M. Liu, L. Jiang, *Nat. Commun.* **2017**, *8*, 15911.

[7] a) Y. Ye, Y. Zhang, Y. Chen, X. Han, F. Jiang, *Adv. Funct. Mater.* **2020**, *30*, 2003430; b) Q. Rong, W. Lei, L. Chen, Y. Yin, J. Zhou, M. Liu, *Angew. Chem., Int. Ed.* **2017**, *56*, 14159.

[8] J. Li, A. D. Celiz, J. Yang, Q. Yang, I. Wamala, W. Whyte, B. R. Seo, N. V. Vasilyev, J. J. Vlassak, Z. Suo, D. J. Mooney, *Science* **2017**, *357*, 378.

[9] a) S. H. M. Söntjens, D. L. Nettles, M. A. Carnahan, L. A. Setton, M. W. Grinstaff, *Biomacromolecules* **2005**, *7*, 310; b) B. Balakrishnan, R. Banerjee, *Chem. Rev.* **2011**, *111*, 4453; c) K. Y. Lee, D. J. Mooney, *Chem. Rev.* **2001**, *101*, 1869.

[10] a) X. P. Morelle, W. R. Illeperuma, K. Tian, R. Bai, Z. Suo, J. J. Vlassak, *Adv. Mater.* **2018**, *30*, 1801541; b) P. Rao, T. Li, Z. l. Wu, W. Hong, X. Yang, H. Yu, T.-W. Wong, S. Qu, W. Yang, *Extreme Mech. Lett.* **2019**, *28*, 43; c) X.-F. Zhang, X. Ma, T. Hou, K. Guo, J. Yin, Z. Wang, L. Shu, M. He, J. Yao, *Angew. Chem., Int. Ed.* **2019**, *58*, 7366.

[11] Z. Liu, Y. Wang, Y. Ren, G. Jin, C. Zhang, W. Chen, F. Yan, *Mater. Horiz.* **2020**, *7*, 919.

[12] C. I. Biggs, T. L. Bailey, G. Ben, C. Stubbs, A. Fayter, M. I. Gibson, *Nat. Commun.* **2017**, *8*, 1546.

[13] a) X. Zhao, F. Chen, Y. Li, H. Lu, N. Zhang, M. Ma, *Nat. Commun.* **2018**, *9*, 3579; b) K. Meister, S. Strazdaite, A. L. DeVries, S. Lotze, L. L. C. Olijve, I. K. Voets, H. J. Bakker, *Proc. Natl. Acad. Sci. U. S. A.* **2014**, *111*, 17732; c) L. Wu, L. Li, M. Qu, H. Wang, Y. Bin, *ACS Appl. Polym. Mater.* **2020**, *2*, 3094; d) W. Wang, Y. Liu, S. Wang, X. Fu, T. Zhao, X. Chen, Z. Shao, *ACS Appl. Mater. Interfaces* **2020**, *12*, 25353.

[14] a) N. Lu, R. Na, L. Li, C. Zhang, Z. Chen, S. Zhang, J. Luan, G. Wang, *ACS Appl. Energy Mater.* **2020**, *3*, 1944; b) D. Ma, X. Wu, Y. Wang, H. Liao, P. Wan, L. Zhang, *ACS Appl. Mater. Interfaces* **2019**, *11*, 41701; c) L. Han, K. Liu, M. Wang, K. Wang, L. Fang, H. Chen, J. Zhou, X. Lu, *Adv. Funct. Mater.* **2018**, *28*, 1704195; d) G. Bai, D. Gao, Z. Liu, X. Zhou, J. Wang, *Nature* **2019**, *576*, 437; e) P. Wei, T. Chen, G. Chen, H. Liu, I. T. Mugaanire, K. Hou, M. Zhu, *ACS Appl. Mater. Interfaces* **2020**, *12*, 3068.

[15] a) Q. Rong, W. Lei, J. Huang, M. Liu, *Adv. Energy Mater.* **2018**, *8*, 1801967; b) H. Chen, X. Ren, G. Gao, *ACS Appl. Mater. Interfaces* **2019**, *11*, 28336; c) J. Wu, Z. Wu, X. Lu, S. Han, B.-R. Yang, X. Gui, K. Tao, J. Miao, C. Liu, *ACS Appl. Mater. Interfaces* **2019**, *11*, 9405; d) Y. Wang, L. Zhang, A. Lu, *ACS Appl. Mater. Interfaces* **2019**, *11*, 41710; e) X. Sui, H. Guo, P. Chen, Y. Zhu, C. Wen, Y. Gao, J. Yang, X. Zhang, L. Zhang, *Adv. Funct. Mater.* **2020**, *30*, 1907986; f) X. Su, H. Wang, Z. Tian, X. Duan, Z. Chai, Y. Feng, Y. Wang, Y. Fan, J. Huang, *ACS Appl. Mater. Interfaces* **2020**, *12*, 29757.

[16] F. Mo, G. Liang, Q. Meng, Z. Liu, H. Li, J. Fan, C. Zhi, *Energy Environ. Sci.* **2019**, *12*, 706.

[17] a) A. Tron, S. Jeong, Y. D. Park, J. Mun, *ACS Sustainable Chem. Eng.* **2019**, *7*, 14531; b) T. Chang, G. Zhao, *Adv. Sci.* **2021**, *8*, 2002425.

[18] a) Y. Wang, Y. Chen, J. Gao, H. G. Yoon, L. Jin, M. Forsyth, T. J. Dingemans, L. A. Madsen, *Adv. Mater.* **2016**, *28*, 2571; b) Y. Ding, J. Zhang, L. Chang, X. Zhang, H. Liu, L. Jiang, *Adv. Mater.* **2017**, *29*, 1704253; c) Y. Ren, J. Guo, Z. Liu, Z. Sun, Y. Wu, L. Liu, F. Yan, *Sci. Adv.* **2019**, *5*, eaax0648; d) F. Chen, D. Zhou, J. Wang, T. Li, X. Zhou, T. Gan, S. Handschuh-Wang, X. Zhou, *Angew. Chem. Int., Ed. Engl.* **2018**, *57*, 6568; e) K. Yang, Y. Wang, Y. You, H. Yang, X. Hao, *Chem. Eng. J.* **2020**, *382*, 122926; f) G. Ge, W. Yuan, W. Zhao, Y. Lu, Y. Zhang, W. Wang, P. Chen, W. Huang, W. Si, X. Dong, *J. Mater. Chem. A* **2019**, *7*, 5949; g) L. Han, K. Liu, M. Wang, K. Wang, L. Fang, H. Chen, J. Zhou, X. Lu, *Adv. Func. Mater.* **2018**, *28*, 1704195; h) C. Hu, Y. Zhang, X. Wang, L. Xing, L. Shi, R. Ran, *ACS Appl. Mater. Interfaces* **2018**, *10*, 44000; i) S. Xia, S. Song, Y. Li, G. Gao, *J. Mater. Chem. C* **2019**, *7*, 11303; j) L. Sun, S. Chen, Y. Guo, J. Song, L. Zhang, L. Xiao, Q. Guan, Z. You, *Nano Energy* **2019**, *63*, 103847; k) K. Wang, J. Wang, L. Li, L. Xu, N. Feng, Y. Wang, X. Fei, J. Tian, Y. Li, *Chem. Eng. J.* **2019**, *372*, 216; l) S. Shi, X. Peng, T. Liu, Y.-N. Chen, C. He, H. Wang, *Polymer* **2017**, *111*, 168; m) Y. Jian, B. Wu, X. Le, Y. Liang, Y. Zhang, D. Zhang, L. Zhang, W. Lu, J. Zhang, T. Chen, *Research* **2019**, *2019*, 2384347; n) J. Liu, C. Xie, A. Kretzschmann, K. Koynov, H. J. Butt, S. Wu, *Adv. Mater.* **2020**, *32*, 1908324.

[19] a) X. P. Morelle, W. R. Illeperuma, K. Tian, R. Bai, Z. Suo, J. J. Vlassak, *Adv. Mater.* **2018**, *30*, e1801541; b) X. F. Zhang, X. Ma, T. Hou, K. Guo, J. Yin, Z. Wang, L. Shu, M. He, J. Yao, *Angew. Chem. Int., Ed. Engl.* **2019**, *58*, 7366; c) X. Sui, H. Guo, P. Chen, Y. Zhu, C. Wen, Y. Gao, J. Yang, X. Zhang, L. Zhang, *Adv. Funct. Mater.* **2020**, *30*, 1907986; d) Y. Liu, J. Yin, Y. Fu, P. Zhao, Y. Zhang, B. He, P. He, *Chem. Eng. J.* **2020**, *382*, 122925; e) J. Wei, G. Wei, Y. Shang, J. Zhou, C. Wu, Q. Wang, *Adv. Mater.* **2019**, *31*, 1900248; f) M. Zhu, X. Wang, H. Tang, J. Wang, Q. Hao, L. Liu, Y. Li, K. Zhang, O. G. Schmidt, *Adv. Funct. Mater.* **2020**, *30*, 1907218.

[20] Y. Ru, R. Fang, Z. Gu, L. Jiang, M. Liu, *Angew. Chem., Int. Ed.* **2020**, *59*, 11876.

[21] T. L. Sun, T. Kurokawa, S. Kuroda, A. B. Ihsan, T. Akasaki, K. Sato, M. A. Haque, T. Nakajima, J. P. Gong, *Nat. Mater.* **2013**, *12*, 932.

[22] A. Romo-Uribe, L. Albanil, *ACS Appl. Mater. Interfaces* **2019**, *11*, 24447.

[23] J. Hao, R. A. Weiss, *Macromolecules* **2011**, *44*, 9390.

[24] M. Chen, J. Chen, W. Zhou, X. Han, Y. Yao, C. P. Wong, *Adv. Mater.* **2021**, *33*, 2007559.

[25] a) X.-H. Li, C. Liu, S.-P. Feng, N. X. Fang, *Joule* **2019**, *3*, 290; b) Y. Zhou, S. Wang, J. Peng, Y. Tan, C. Li, F. Y. C. Boey, Y. Long, *Joule* **2020**, *4*, 2458.
[26] Q. Chen, L. Zhu, C. Zhao, Q. Wang, J. Zheng, *Adv. Mater.* **2013**, *25*, 4171.
[27] M. Zhang, D. Zhang, H. Chen, Y. Zhang, Y. Liu, B. Ren, J. Zheng, *npj Computational Materials* **2021**, *7*, 39.
[28] A. D. MacKerell Jr, D. Bashford, M. Bellott, R. L. Dunbrack Jr., J. D. Evanseck, M. J. Field, S. Fischer, J. Gao, H. Guo, S. Ha, *J. Phys. Chem. B* **1998**, *102*, 3586.
[29] J. C. Phillips, R. Braun, W. Wang, J. Gumbart, E. Tajkhorshid, E. Villa, C. Chipot, R. D. Skeel, L. Kale, K. Schulten, *J. Comput. Chem.* **2005**, *26*, 1781.
[30] W. Humphrey, A. Dalke, K. Schulten, *J. Mol. Graph.* **1996**, *14*, 33.